

Investigating the morphology of the supernova remnant G349.7+00.2 in the medium with a density gradient

Jing-Wen Yan (严婧雯)¹, Chun-Yan Lu (卢春燕)¹, Lu Wen (问璐)¹, Huan Yu (于欢)² and Jun Fang (方军)^{1,3}

¹ Department of Astronomy, Key Laboratory of Astroparticle Physics of Yunnan Province, Yunnan University, Kunming 650091, China; fangjun@ynu.edu.cn

² Department of Physical Science and Technology, Kunming University, Kunming 650214, China; yuhuan.0723@163.com

³ Institute of High Energy Physics, Chinese Academy of Sciences, Beijing 100049, China

Received 2020 February 20; accepted 2020 April 21

Abstract G349.7 + 00.2 is a young Galactic supernova remnant (SNR) with a mushroom morphology in radio and X-rays, and it has been detected across the entire electromagnetic spectrum from radio to high energy γ -rays. Moreover, the remnant is interacting with a molecular cloud based on the observations in the radio and infrared band. The reason for the formation of the periphery and the dynamical evolution of the remnant is investigated using 3D hydrodynamical (HD) simulations. Under the assumption that the supernova ejecta is evolved in the medium with a density gradient, the shell is composed of two hemispheres with different radii, and the smaller hemisphere is in relatively dense media. The resulting periphery of remnant is consistent with detected ones, and it can be concluded that the peculiar periphery of G349.7+00.2 can be reproduced as the remnants interacting with the medium with a density gradient.

Key words: hydrodynamics (HD) — methods: numerical — ISM: supernova remnants

1 INTRODUCTION

Supernova remnants (SNRs) are the candidate of the primary accelerators of the Galactic cosmic rays, and the dynamical evolution and the morphology of them heavily depend on the properties of the ambient medium (e.g., Reynolds 2008; Fang et al. 2019; Zeng et al. 2019). For example, SNR G349.7+00.2, which has a distance of 22 kpc and the age of 2800 yr based on the observations of H_I absorption (Caswell et al. 1975), 1720 MHz OH masers (Frail et al. 1996) and CO (Reynoso & Mangum 2000), has a peculiar morphology as indicated in radio and X-rays. The radio image is characterized by a distinct brightness enhancement along the southeastern limb, where the remnant is interacting with a molecular cloud. The radio structure can be fitted by two overlapping rings, with one smaller and brighter than the other, this feature can be considered that a smaller ring corresponds to a higher density of the inflated shell (Manchester 1988). In X-rays, G349.7+0.2 was first detected in the Galactic plane survey of ASCA (Yamauchi et al. 1998). The analysis of the ASCA data (Slane et al. 2002) showed that the spec-

trum was well fit by a single-temperature non-equilibrium ionization mode. The Chandra observations also revealed a compact central object inside the SNR shell, called CXOUJ171801.0–372617. The X-ray brightness is enhanced in the southeastern limb, and the overall morphology is similar to that observed in the radio (Lazendic et al. 2005).

The peculiar morphology of G349.7+00.2 shed light on the ambient medium. Reynoso & Mangum (2000) proposed that the shock front of the remnant has been extended to the density gradient, and the smaller half of the shell has been expanded to a higher density of gas. Moreover, CO observations toward G349.7+0.2 also revealed a molecular cloud associated with the SNR (Reynoso & Mangum 2000; Reynoso & Mangum 2001; Lazendic et al. 2002b). Five OH (1720 MHz) maser spots were found in the center of the SNR (Frail et al. 1996), and the shock-excited near-infrared H_I emission has been found toward the center of the remnant as well as OH absorption (1665 and 1667 MHz) in the remnant (Lazendic et al. 2002a). The line emission from several molecular transitions shows clear evidence of in-

teraction between the SNR and the molecular clouds (MCs) (Reynoso & Mangum 2000; Lazendic et al. 2002a; Dubner et al. 2004).

Ergin et al. (2015) analyzed the GeV γ -rays from G349.7+0.2 and found that the detected spectrum can be represented by a broken power law distribution of $\alpha = 1.89$ and $\beta = 2.42$ and a spectral break at 12 GeV. Zhang et al. (2016) constrained the parameters of the escaping-diffusion model using the Markov Chain Monte Carlo method, and they found that the correction factor of slow diffusion around this SNR; i.e., $\chi = 0.01$ for the power-law injection and $\chi = 0.1$ for the δ -function injection. The γ -ray spectrum can be fit with a reasonable molecular cloud mass. In addition, Hnatyk & Petruk (1999) performed 2D hydrodynamical modeling of the evolution and X-ray emission of SNRs expanding in a large-scale density gradient, and the results showed that the remnant expanded into a density gradient.

Three-dimensional (3D) hydrodynamic/ magnetohydrodynamic (HD/ MHD) simulations are widely used to study the morphologies of SNRs (Toledo-Roy et al. 2014; Fang et al. 2017, 2018, 2020). In this paper, we investigate the reason for the formation of the periphery of G349.7+00.2 using 3D HD simulation under the assumption that the supernova ejecta is evolved in the medium with a density gradient. A detailed description of our model and initial setup of simulations are described in Section 2. The results are presented in Section 3, and some discussion and conclusions are given in Section 4.

2 SIMULATION SETUP

In order to investigate the dynamical evolution of the remnant G349.7+00.2 and reproduce the special morphology, we adopt 3D HD numerical simulations on it with the Pluto code (Mignone et al. 2007, 2012), which provides a variety of hydrodynamic modules and algorithms for solving a complete set of MHD/HD equations with different geometry systems. In our simulations, Cartesian geometry (x, y, z) and a computational cube of $6 \times 6 \times 6 \text{ pc}^{-3}$ with $512 \times 512 \times 512$ grids are used.

We assume that the ejecta of G349.7+00.2 has evolved in the nonuniform medium with a density gradient, which directs along $\hat{\xi} = \sin \theta \cos \phi \hat{e}_x + \sin \theta \sin \phi \hat{e}_y + \cos \theta \hat{e}_z$. After the supernova explosion, the ejecta has a mass of $M_{\text{ej}} = 8.0 M_{\odot}$, a kinetic energy of $E_{\text{ej}} = 10^{51} \text{ erg}$ and a radius of $R_{\text{ej}} = 0.5 \text{ pc}$, which is set at the center of the simulation. The initial matter distribution for the ejecta includes an inner core having a constant density ρ_c within the r_c radius, and an outer layer with a power-law density

profile (Fang et al. 2020); i.e.,

$$\rho_{\text{ej}}(r) = \begin{cases} \rho_c, & \text{if } r < r_c, \\ \rho_o(r/R_{\text{ej}})^{-S}, & \text{if } r_c < r < R_{\text{ej}}, \end{cases} \quad (1)$$

where ρ_o is the density at $r = R_{\text{ej}}$. η is the mass ratio of the outer part of the ejecta to the inner one. The index $S = 9$ is used in this paper for the core-collapse supernova explosion. The density of the inner core is (Jun & Norman 1996)

$$\rho_c = \frac{3(1-\eta)M_{\text{ej}}}{4\pi r_c^3}. \quad (2)$$

Moreover, r_c can be obtained with

$$r_c = R_{\text{ej}} \left[1 - \frac{\eta(3-S)M_{\text{ej}}}{4\pi\rho_o R_{\text{ej}}^3} \right]^{1/(3-S)}. \quad (3)$$

The velocity of the matter in the ejecta at r is $v = \frac{r}{R_{\text{ej}}} v_0$ for $r \leq R_{\text{ej}}$. The velocity of ejecta at the outer edge v_0 can be obtained by

$$v_0 = (E_{\text{ej}})^{\frac{1}{2}} \left\{ \frac{2\pi\rho_c r_c^5}{5R_{\text{ej}}^2} + \frac{2\pi\rho_o R_{\text{ej}}^3 [1 - (R_{\text{ej}}/r_c)^{S-5}]}{5-S} \right\}^{-1/2}. \quad (4)$$

Assuming that the ejection evolved in an environmental medium with a density gradient, the number density of environmental media satisfies the following formula,

$$n(\mathbf{r}) = \begin{cases} n_0 + k\hat{\xi} \cdot \mathbf{r}, & \text{if } \hat{\xi} \cdot \mathbf{r} > 0, \\ n_0, & \text{otherwise,} \end{cases} \quad (5)$$

where k is the magnitude of the density gradient. $\mu = 1.4$ is the mean atomic mass for a gas of a 10 : 1 H:He ratio.

Neglecting the radiative cooling and the particle acceleration involved in the remnant, the dynamical properties of the ejecta can be simulated based on the Euler equations, i.e.

$$\frac{\partial \rho}{\partial t} + \nabla \cdot (\rho V) = 0, \quad (6)$$

$$\frac{\partial \rho V}{\partial t} + \nabla \cdot (\rho V V) + \nabla P = 0, \quad (7)$$

$$\frac{\partial E}{\partial t} + \nabla \cdot (E + P)V = 0, \quad (8)$$

and

$$E = \frac{P}{\gamma - 1} + \frac{1}{2}\rho V^2, \quad (9)$$

where P and E are the gas pressure and the total energy density, respectively. $\gamma = 5/3$ is adopted for the nonrelativistic gas and V is the gas velocity.

Table 1 Parameters for the modes with different polar angles (θ) and different azimuth angles (ϕ) with $E_{\text{ej}} = 10^{51}$ erg, $R_{\text{ej}} = 0.5$ pc, $M_{\text{ej}} = 8.0 M_{\odot}$, $n_0 = 10 \text{ cm}^{-3}$, $k = 50 \text{ cm}^{-3} \text{ pc}^{-1}$.

Parameter	mode A	mode B	mode C	mode D	mode E	mode F
$\theta(^{\circ})$	60	120	200	120	120	60
$\phi(^{\circ})$	250	250	250	60	180	300

Table 2 Parameters for the different modes in the simulations. The common parameters are $E_{\text{ej}} = 10^{51}$ erg, $R_{\text{ej}} = 0.5$ pc, $M_{\text{ej}} = 8.0 M_{\odot}$, $n_0 = 10 \text{ cm}^{-3}$, $\theta = 120^{\circ}$ and $\phi = 250^{\circ}$.

Parameter	mode H	mode I	mode J	mode K	mode L
($k \text{ cm}^{-3} \text{ pc}^{-1}$)	8	15	25	30	40

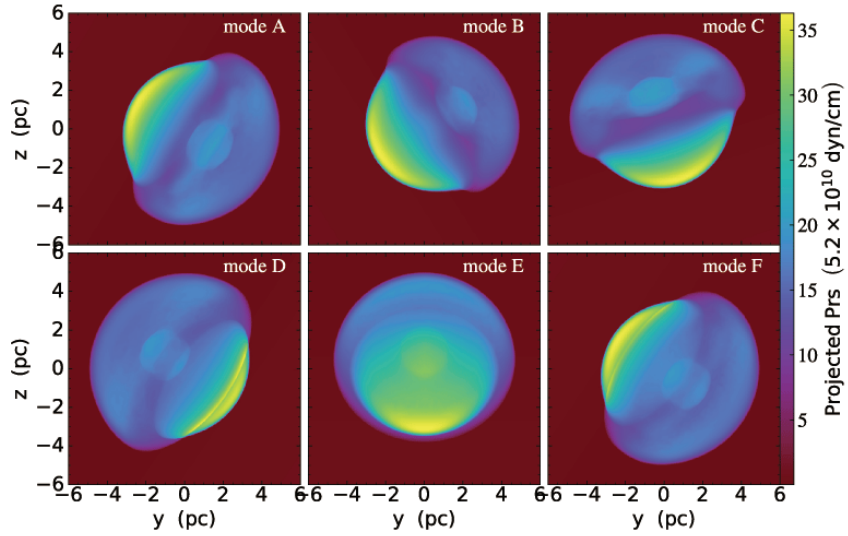


Fig. 1 The projected pressure along the x direction at $t = 2800$ yr for modes A - F with different polar angles (θ) and azimuth angles (ϕ). The other parameters are $E_{\text{ej}} = 10^{51}$ erg, $R_{\text{ej}} = 0.5$ pc, $M_{\text{ej}} = 8.0 M_{\odot}$, $n_0 = 10 \text{ cm}^{-3}$, $k = 50 \text{ cm}^{-3} \text{ pc}^{-1}$.

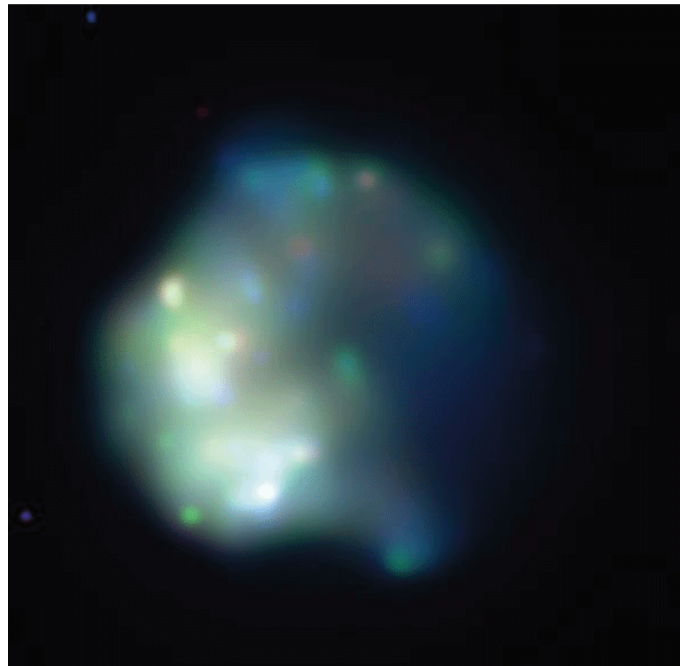


Fig. 2 The observed X-ray morphology of SNR G349.7+00.2 with Chandra. This image is adopted from the website <http://hea-www.harvard.edu/ChandraSNR/gallerygal.html>.

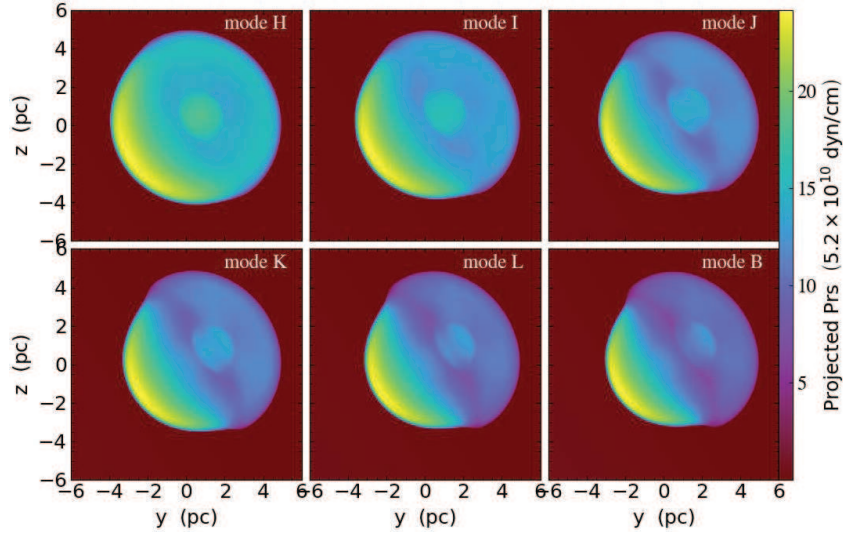


Fig. 3 The projected pressure along the x direction at $t = 2800$ yr for modes H - L and mode B. The common parameters are $E_{\text{ej}} = 10^{51}$ erg, $R_{\text{ej}} = 0.5$ pc, $M_{\text{ej}} = 8.0 M_{\odot}$, $n_0 = 10 \text{ cm}^{-3}$, $\theta = 120^\circ$ and $\phi = 250^\circ$.

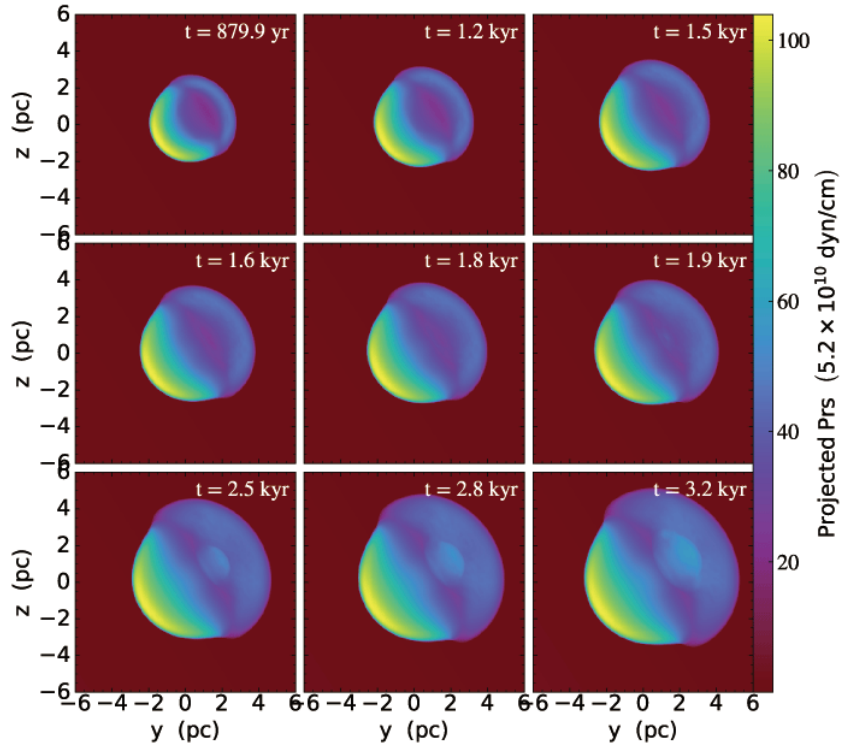


Fig. 4 The evolution of the projected pressure along the x direction at different times for mode B. The other parameters are the same as Fig. 3.

3 RESULTS

G349.7 + 00.2 has a peculiar and interesting morphology in the radio and X-rays, and we intend to study the periphery of SNR G349.7 + 00.2 through studying the effect of different density gradients. We assume that there is a density gradient in the ambient medium directed along

$\hat{\xi} = \sin \theta \cos \phi \hat{e}_x + \sin \theta \sin \phi \hat{e}_y + \cos \theta \hat{e}_z$. Firstly, n_0 is set to 10 cm^{-3} based on the studies in [Tian & Leahy \(2014\)](#). With $M_{\text{ej}} = 8.0 M_{\odot}$, $E_{\text{ej}} = 10^{51}$ erg can lead to a radius consistent with the observations, so we adopt these values in the simulations. As listed in [Table 1](#), the six modes with different combinations are calculated to seek a reasonable

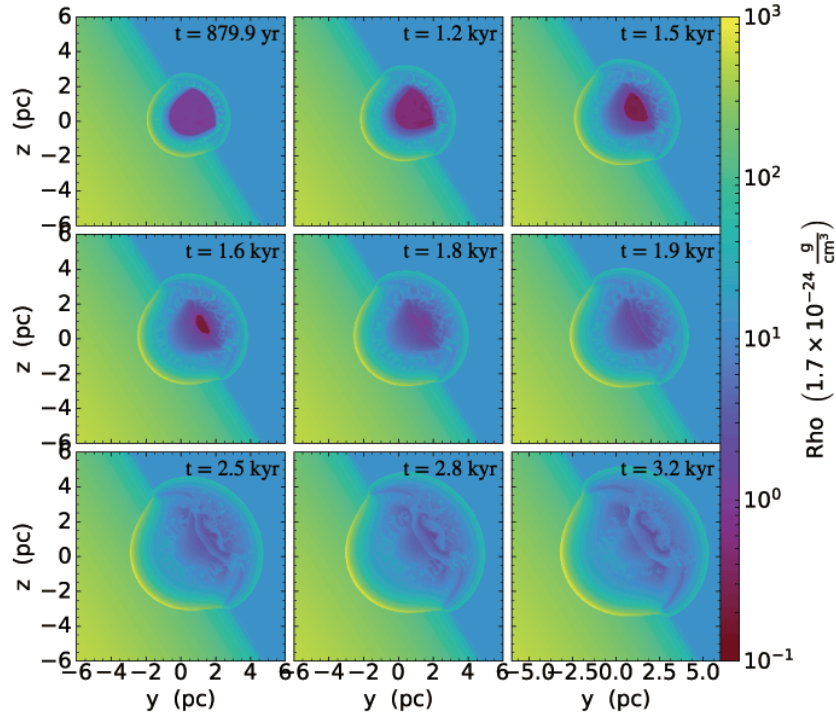


Fig. 5 The slices of the density in the plane $x = 0$ at $t = 2800$ yr for mode B. The other parameters are the same as Fig. 3.

polar angle θ and an azimuth angle ϕ to reproduce the detected periphery of the remnant.

Figure 1 shows the morphologies of the projected pressure along the x direction at $t = 2800$ yr for these different polar angles θ and the azimuth angles ϕ . With $\theta = 120^\circ$ (modes B, D, and E), the morphology is not found to be composed of two hemispheres with an azimuth angle much less than 180° as illustrated in mode D. The influence of the polar angle on the resulting morphology of the projected pressure can be seen in the upper three panels (modes A - C) with $\phi = 250^\circ$, and that with $\theta \sim 120^\circ$ can be constrained by the image detected by Chandra (Fig. 2).

Figure 3 shows the morphologies of the projected pressure along the x direction for the modes with different density gradient as listed with $\theta = 120^\circ$ and $\phi = 250^\circ$. The details of the parameters for modes H - L and B and are shown in Table 2. All these modes can produce morphologies with two hemispheres. The radius of the hemisphere in the denser medium becomes smaller for a larger density gradient with a deeper hollow between the two hemispheres. Compared with the detected image with Chandra, the density gradient of $30 - 50 \text{ cm}^{-3} \text{ pc}^{-1}$ can reproduce a consistent periphery.

Figure 4 shows the morphologies of the projected pressure along the x direction at different times for mode B, and the slices of density at the plane $x = 0$ are indicated in Figure 5. Initially, in the two hemispheres, the forward shocks are produced due to the supersonic motion of the

ejecta. As the forward shock expands outwardly, the material in the inner part of the remnant becomes tenuous until the thermalized medium drives a reverse shock which continually compresses the matter in the ejecta. As illustrated in the panel for $t = 1.2$ kyr in Figure 4, the reverse shock marks the boundary of the low-density ejecta in the center of the remnant. Due to the Rayleigh-Taylor instabilities, the fingertip structure is produced near the contact discontinuity. At a time of 2.5 kyr, the reverse shocks from the two hemispheres had encountered with each other near the center of the remnant. On the other hand, the pressure in the southeast (SE) area of the remnant becomes more significant than the other areas due to the higher density. For mode B, at a time of $t = 2800$ yr, the forward shock in the denser medium has a radius of ~ 3.0 pc, whereas it is ~ 3.4 pc in the other hemisphere, which is consistent with the image obtained with Chandra for a distance of 22 kpc.

4 SUMMARY AND DISCUSSION

G349.7+00.2 has a peculiar morphology in the X-rays. The dynamical evolution and the morphology of an SNR heavily depend on the anisotropy and inhomogeneity of both the ejecta and the ambient medium. In this paper, we investigate the reason for the formation of the peculiar periphery as indicated in the observations for the SNR G349.7+00.2 based on 3D HD simulation. In the model, we assume that the ejecta of G349.7+00.2 has evolved in the ambient medium with a density gradient. The shell consists of t-

two hemispheres with different radii, and the resulting morphology of the projected pressure varies with different density gradients. Moreover, the peculiar periphery illustrated in the detected images can be reproduced with the model.

With a distance of 22 kpc, the main shell of SNR G349.7+00.2 has two different hemispheres with a radius ratio of about 1 : 1.13 based on the observed image by Chandra, which is consistent with mode B at the time of 2800 yr with $E_{\text{ej}} = 10^{51}$ erg, $M_{\text{ej}} = 8.0 M_{\odot}$ and $n_0 = 10 \text{ cm}^{-3}$. With $\theta = 120^\circ$ and $\phi = 250^\circ$, we find the resulting profile of the remnant in mode B is similar to that in the X-ray image. Therefore, $k = 50 \text{ cm}^{-3} \text{ pc}^{-1}$ is suitable to explain the special morphology of SNR G349.7+00.2 and our results support the assumption of the mode. The X-ray image is characterized by a distinct brightness enhancement along the southeastern limb, which are illustrated in the image of the projected pressure. Moreover, the shell in the northeast is bright in the X-ray image. Our numerical simulation results show that the bright ridge can be explained as the ejecta interacting with the medium with a higher density.

G349.7+00.2 is one of the radio and X-ray brightest SNRs in the Galaxy, and there is much evidence that it is interacting with molecular clouds. Through the analysis of the gamma-ray data, it is considered that G349.7+0.2 is expanding in a dense medium of molecular clouds and emitting gamma-rays by interacting with clumps of molecular material (Ergin et al. 2015). Previous research has claimed that the surrounding molecular gas caused the peculiar morphologies (Lazendic et al. 2005; Castro & Slane 2010). Alternatively, Yasumi et al. (2014) proposed that asymmetric explosions could produce such morphologies. In this paper, we assume that this morphology is due to the evolution of the ejecta in a medium with a density gradient, and use 3D HD simulation to reproduce its special periphery.

Acknowledgements JF is partially supported by the National Natural Science Foundation of China (NSFC, No. 11873042), the Yunnan Applied Basic Research Projects (2018FY001(-003)), the National Key R&D Program of China (No.2018YFA0404204), the Candidate Talents Training Fund of Yunnan Province (2017HB003) and the Program for Excellent Young Talents, Yunnan University (WX069051 and 2017YDYQ01).

References

- Castro, D., & Slane, P. 2010, *ApJ*, 717, 372
- Caswell, J. L., Murray, J. D., Roger, R. S., Cole, D. J., & Cooke, D. J. 1975, *A&A*, 45, 239
- Dubner, G., Giacani, E., Reynoso, E., & Parón, S. 2004, *A&A*, 426, 201
- Ergin, T., Sezer, A., Saha, L., et al. 2015, *ApJ*, 804, 124
- Fang, J., Yu, H., & Zhang, L. 2017, *MNRAS*, 464, 940
- Fang, J., Yu, H., & Zhang, L. 2018, *MNRAS*, 474, 2544
- Fang, J., Lu, C.-Y., Yan, J.-W., & Yu, H. 2019, *RAA (Research in Astronomy and Astrophysics)*, 19, 182
- Fang, J., Yan, J., Wen, L., Lu, C., & Yu, H. 2020, *MNRAS*, 491, 2460
- Frail, D. A., Goss, W. M., Reynoso, E. M., et al. 1996, *AJ*, 111, 1651
- Hnatyk, B., & Petruk, O. 1999, *A&A*, 344, 295
- Jun, B.-I., & Norman, M. L. 1996, *ApJ*, 465, 800
- Lazendic, J. S., Wardle, M., Burton, M. G., et al. 2002a, *MNRAS*, 331, 537
- Lazendic, J. S., Wardle, M., Green, A. J., Whiteoak, J. B., & Burton, M. G. 2002b, in *Astronomical Society of the Pacific Conference Series*, 271, *Neutron Stars in Supernova Remnants*, eds. P. O. Slane, & B. M. Gaensler, 399
- Lazendic, J. S., Slane, P. O., Hughes, J. P., Chen, Y., & Dame, T. M. 2005, *ApJ*, 618, 733
- Manchester, R. N. 1988, in *Proceedings of the Astronomical Society of Australia*, 7, 548
- Mignone, A., Bodo, G., Massaglia, S., et al. 2007, *ApJS*, 170, 228
- Mignone, A., Zanni, C., Tzeferacos, P., et al. 2012, *ApJS*, 198, 7
- Reynolds, S. P. 2008, *ARA&A*, 46, 89
- Reynoso, E. M., & Mangum, J. G. 2000, *ApJ*, 545, 874
- Reynoso, E. M., & Mangum, J. G. 2001, *AJ*, 121, 347
- Slane, P., Chen, Y., Lazendic, J. S., & Hughes, J. P. 2002, *ApJ*, 580, 904
- Tian, W. W., & Leahy, D. A. 2014, *ApJL*, 783, L2
- Toledo-Roy, J. C., Esquivel, A., Velázquez, P. F., & Reynoso, E. M. 2014, *MNRAS*, 442, 229
- Yamauchi, S., Koyama, K., Kinugasa, K., et al. 1998, *Astronomische Nachrichten*, 319, 111
- Yasumi, M., Nobukawa, M., Nakashima, S., et al. 2014, *PASJ*, 66, 68
- Zeng, H., Xin, Y., & Liu, S. 2019, *ApJ*, 874, 50
- Zhang, X., Li, H., & Chen, Y. 2016, *RAA (Research in Astronomy and Astrophysics)*, 16, 152